AERODYNAMIC OPTIMIZATION OF A MORPHING MEMBRANE WING

B. Béguin*, C. Breitsamter*, N. Adams*
***Institute of Aerodynamics and Fluid Mechanics, Technische Universität München**
benoit.beguin@aer.mw.tum.de, christian.breitsamter@aer.mw.tum.de, nikolaus.adams@tum.de

Keywords: *Applied aerodynamics, morphing wing, membrane wing, experimental methods*

Abstract

This paper considers a morphing membrane wing concept capable of achieving large variations of the planform and airfoil shapes. Due to its high flexibility, the wing surface deforms under aerodynamic load and, as a result, the aerodynamic characteristics show a passive dependency on the flow conditions.
The current investigations focus on the possibility to control the passive deformation of the membrane by actively varying its pre-tension. For this, experimental tests including force and deformation measurements are performed on a wind tunnel model using a movable trailing-edge to modify the pre-tension of the membrane. The results show that this method effectively allows adjusting the camber of the wing within a certain range at a given flow condition, which in turn can be used to positively influence its aerodynamic performances.

1 Introduction

In the context of aircraft design, morphing describes the ability of a vehicle to achieve seamless changes of its outer shape in order to alter its performance characteristics. This would allow a single aircraft to achieve different mission roles efficiently and effectively. Even if the benefits of morphing are obvious for the aerodynamicist, technical realizations are still a critical issue. In fact, new challenges concerning the design methods, materials, actuators and flight control have to be mastered in order that the improved aerodynamics created by wing morphing effectively offsets the penalties due to the additional weight and energy consumption used to physically morph the vehicle [1].
While considering morphing technologies, it can be differentiated between *active* and *passive* morphing. In the case of the *active* morphing, the energy required to actuate the structure and achieve a predefined shape change must be available in the vehicle [2], [3]. In the case of the *passive* morphing, the aerodynamic forces are used to deform the structure and thus, the energy is taken from the air flow. This type of morphing requires specific structural characteristics in order to achieve a predefined shape change at a given load. Passive morphing is an attractive method to achieve lightweight structure and when small scale geometry variations have to be achieved. The NASA's Active Aeroelastic Wing project illustrates an application of passive morphing technology [4].

2 The Morphing Membrane Wing

2.1 Description

The morphing wing concept considered in this paper uses an articulating inner structure over which a compliant membrane is spanned to form the actual aerodynamic surface. This particular construction allows achieving large variations of the planform with reasonable actuation energy while ensuring a seamless aerodynamic surface.

While the planform configuration can be actively morphed through the actuation of the articulating inner structure, the highly flexible wing surface deforms passively under aerodynamic load and as a result the wing camber depends on the flow conditions.
A half-wing wind tunnel model with a maximum span of b = 1 m has been designed and build for the experimental investigations of this concept (Fig. 1). The different segments constituting the leading-edge of the articulating structure are connected together using linkages such that the whole structure can be actuated via a single stepper motor. With the current design, the planform can be continuously varied between a high aspect ratio, straight-wing and a low aspect ratio, swept-back configuration. The leading-edge spar has an asymmetric cross section (Fig. 1c) in order to obtain smoother pressure distribution compared to a simpler rounded spar [5]. The trailing-edge consists of a telescopic spar which length adapts to the current configuration. The membrane material currently used (provided by *Eschler Textil GmbH*) consists of a 0.5 mm thick elastic fabric coated on one side with a rubber layer ensuring air impermeability. For the wing surface, a cover with an appropriate cut is sewed out of this membrane material and comes wrapped around the inner structure. The fabric has anisotropic structural characteristics and for the wing surface, the stiffer direction is roughly aligned with the chord of the wing.

2.2 Background: Results of Previous Investigations

Here, the basic characteristics of this morphing wing concept obtained from previous experimental investigations [6] are presented in order to provide some background and motivation for the work presented later in this paper. The main characteristic of the wing is the pronounced dependency of its aerodynamic properties on the flow condition coming from the passive deformation of the wing surface, as illustrated in Fig. 2. At low free-stream dynamic pressures, the wing behaves mostly like a conventional rigid wing with

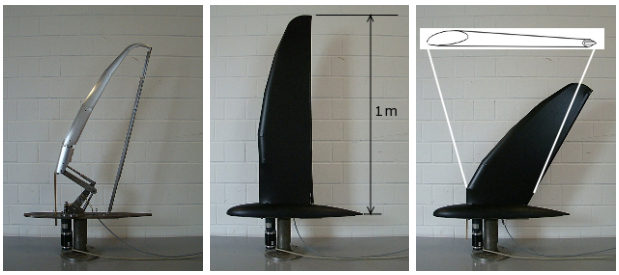

(a) (b) (c)

Fig. 1 Morphing wind tunnel model. a) Inner articulating structure, b) Complete wing in the straight-wing configuration, c) Swept-back configuration with a schematic visualization of a wing section.

a linear lift curve accordingly to the small deformation. At higher free-stream dynamic pressure, the increasing amplitude of the deformation leads to non-linear characteristics with a larger slope of the lift curve because the camber of the wing significantly varies with the angle of attack. Further, this passive adaption of the camber acts like a natural flow control mechanism leading to delayed and smoother stall characteristics (Fig. 2b).
Despite this unconventional behavior, the comparison of the aerodynamic characteristics measured on different wing configurations shows that morphing the wing planform still alters the lift and drag characteristics as expected from rigid wing theory. For instance, Fig. 2c illustrates the influence of morphing the wing planform on the lift-to-drag ratio, showing that it effectively leads to an aerodynamic benefit since the range of optimum L/D values can be expanded by morphing the wing planform. The passive camber morphing just shifts the characteristics as the free-stream dynamic pressure changes.

2.3 Controlling the Passive Morphing

As illustrated in Fig. 2a, the passive morphing results in small wing cambers at low free-steam dynamic pressures, and in large wing cambers at higher dynamic pressures, because the membrane reacts passively to a variation of the aerodynamic loading. However, this tendency is the opposite to what one would expect from a morphing air-

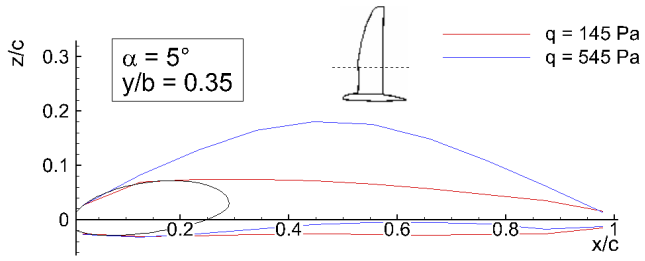

(a) Airfoil shapes obtained from stereo-photogrammetry measurements.

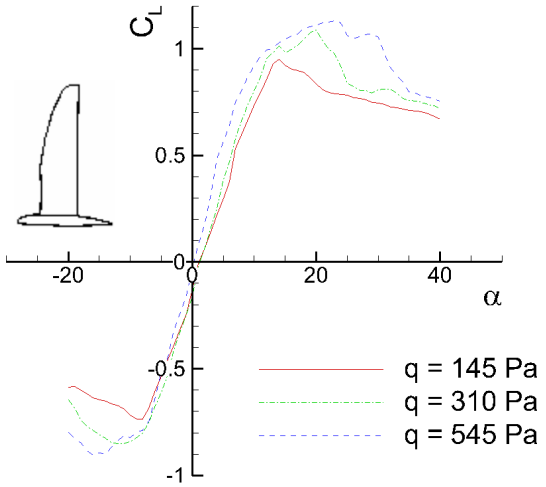

(b) Lift characteristics.

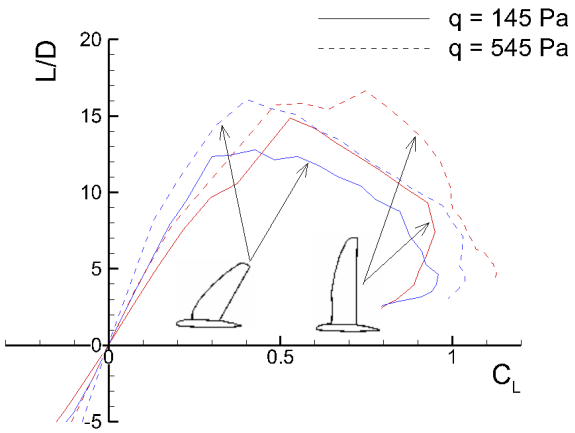

(c) Influence of the wing configuration and flow condition on the lift-to drag ratio.

Fig. 2 Experimental results from previous investigations.

foil since large cambers are known to be advantageous at low flight speed and vice versa.
The solution investigated in this paper to control the passive morphing proposes to modify actively the pre-tension of the membrane to control the amplitude of the deflection within a certain range at a given aerodynamic loading. In order to inves-

Fig. 3 Illustration showing the movable trailing-edge of the wind tunnel model (here in the swept-back planform configuration). The root chord length c_r can be varied between 0.24 and 0.27 m.

tigate this, the basis wind tunnel model has been modified to allow for a variation of the position of the attachment point of the trailing-edge at the root of the wing as shown in Fig. 3. The resulting modification of the chord length affects the pre-tension of the membrane accordingly. The plots of Fig. 4 show the geometrical characteristics of the wing in terms of the planform area (S_{ref}) and aspect ratio (AR) as function of the sweep angle Λ_{LE} and root chord length c_r . Even if the main purpose of moving the trailing-edge is to influence the pre-tension of the membrane, it also slightly modifies the planform area.

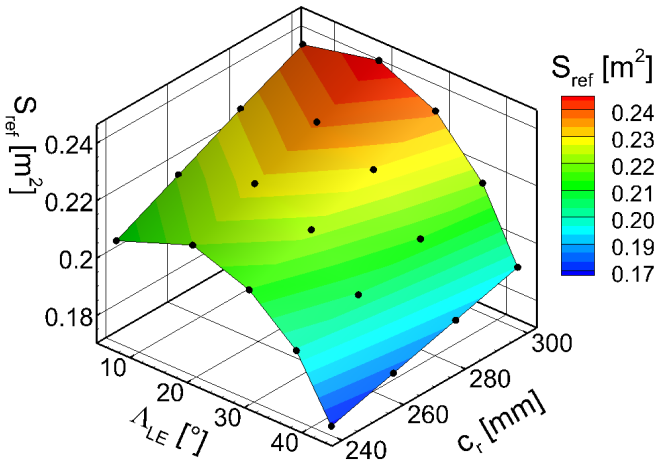

(a) Planform area S_{ref}.

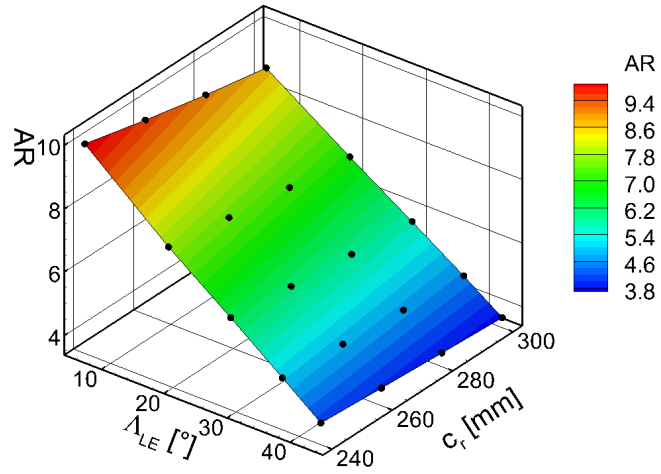

(b) Aspect ratio AR.

Fig. 4 Geometric characteristics of the wing planform. The black dots indicate the wing configurations which were tested experimentally.

3 Experimental Methods and Setups

The morphing wing model presented above was tested in the low-speed wind tunnel facility A at the Institute of Aerodynamics and Fluid Mechanics of the Technische Universität München. This wind tunnel has a 4.8 m long, open test section with a rectangular section of 1.8 m in height by 2.4 m in width. It generates wind speeds up to 65 m/s with free-stream turbulence level below 0.4%.

The tests included stereo-photogrammetry measurements to analyze the wing geometries resulting from the deformation of the wing surface, and force measurements to assess the overall aerodynamic characteristics of the wing.

For the force measurements, the wing model was fixed to an external six-components aerodynamic balance located under the floor of the wind tunnel's test section. In order to avoid interaction of the model with the boundary layer developing on the floor, the model is elevated by 130 mm and a peniche is used to cover the portion of the fixation shaft exposed to the airflow (Fig. 5). Finally, time averaged forces over 20 seconds were recorded for all measurement points described in Tab. 1.

For the stereo-photogrammetry, two *Flow Sense 2M* cameras with a resolution of 1600 $\times$ 1200 pixels were used. Due to the imaging optics used (Nikkor-objective with a focal length of 135 mm) and the distance to the model, only an area of 240 $\times$ 180 mm can be measured with an average spatial resolution of 0.15 mm per pixel. For this reason, a traversing system was used to move the cameras and allow the reconstruction of a significant portion of the wing. However, the travel distance available was not yet sufficient to measure the complete wing, such that a portion at the root (below y/b = 0.2) and at the tip (above y/b = 0.9) could not be measured. A self developed code implementing the Direct Linear Transformation method [7] was used to reconstruct the 3-dimensional coordinates of 230 markers placed on each wing surface (see Fig. 5). Measurements were performed on both the upper and the lower side of the wing in order to analyze the complete wing geometry. The results of the camera calibration indicated an average measurement uncertainty below 0.09 mm.

Table 1 presents the test conditions in terms of free-steam dynamic pressure q and angle of attack α. Table 2 indicates the tested wing configurations and the type of measurements performed in each case.

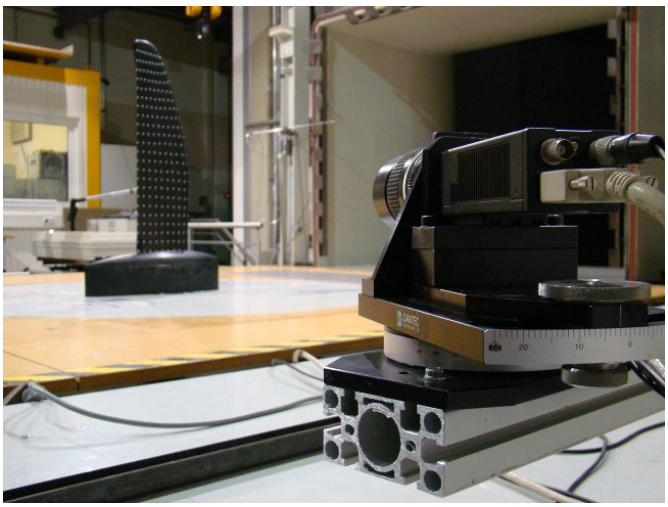

Fig. 5 Picture showing the experimental setup.

	Force meas.	Deflection meas.
q [Pa]	145, 310, 545	145, 310, 545
α [°]	-20→30, 1° incr.	0,5,10

Table 1 Test matrix showing the flow conditions in terms of the free-stream dynamic pressure q and the angle of attack range α.

		Λ_{LE}				
		6°	20°	30°	37°	43°
c_r	0.24 m	F,S	F	F,S	F	F,S
	0.26 m	F,S	F	F,S	F	F,S
	0.28 m	F,S	F	F,S	F	F,S
	0.30 m	F,S	F	F,S	F	F,S

Table 2 Test matrix showing the configurations investigated and the type of measurements performed in each case. F = force measurements, S = stereo-photogrammetry.

4 Results and Discussion

4.1 Pre-tension of the Membrane

The pre-tension of the membrane cannot be measured directly at this stage but its initial deformation (without aerodynamic load) can be precisely measured using the photogrammetry and gives a good approximation of how the pre-tension is expected to vary. The local strain of the membrane is obtained by analyzing the deformation of the

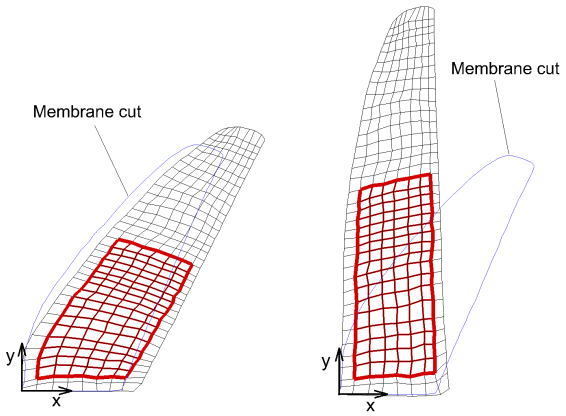

(a) Swept-back conf. (b) Straight-wing conf.

Fig. 6 Illustration from measurements of the initial deformation of the membrane (without aerodynamic load, here with $c_r = 0.24$).

grid cells formed by the array of markings compared to the undeformed membrane (see Fig. 6). Further, the pre-strain is split into its chordwise and spanwise components $\varepsilon_{x,0}$ and $\varepsilon_{y,0}$, respectively. Here the general definition of the pre-strain is $\varepsilon_0 = \frac{l-l_0}{l}$ where l_0 and l represents the dimension of the reference and deformed cell, respectively.

The diagram of Fig. 7 shows the variation of the two components of the local strain $\varepsilon_{x,0}$ and $\varepsilon_{y,0}$ as function of the planform configuration (Λ_{LE}) and the root chord length (c_r). The values given in this diagram come from measurements performed on the lower side of the wing (without aerodynamic load) and are averaged over all the data contained within the red boundary shown in Fig. 6. The spanwise component of the pre-strain, $\varepsilon_{y,0}$, decreases as Λ_{LE} increases according to the variation in wing span. The variation of $\varepsilon_{x,0}$ is due to two distinct influences. On the one hand, there is a significant dependency of $\varepsilon_{x,0}$ on the planform shape, which is due to the intrinsic variation of the chord length while the planform changes. On the other hand, increasing the root chord leads to an increases of $\varepsilon_{x,0}$ as expected.
The values of $\varepsilon_{x,0}$ and $\varepsilon_{y,0}$ interpolated for c_r = 0.27m are also given in Fig. 7, which corresponds to the fixed root chord length used in the

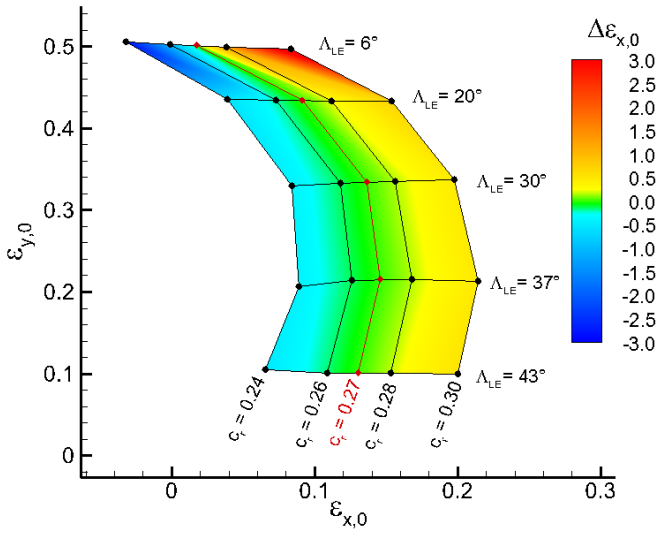

Fig. 7 Pre-strain of the membrane (without aerodynamic load) as function of the planform configuration and root chord length.

		c_r [m]			
		0.24	0.26	0.28	0.3
Λ_{LE} [°]	6	-2.82	-1.05	1.18	3.76
	20	-0.57	-0.2	0.22	0.68
	30	-0.38	-0.14	0.15	0.47
	37	-0.39	-0.14	0.15	0.47
	43	-0.5	-0.17	0.17	0.53

Table 3 Values of $\Delta\varepsilon_{x,0}(c_r)$ for all configurations.

previous version of the wind tunnel model (see Fig. 1). Using these values as reference, the relative variation in $\varepsilon_{x,0}$ achieved by moving the trailing-edge is given for each configuration as follows:

$$\Delta\varepsilon_{x,0}(c_r) = \frac{\varepsilon_{x,0}(c_r) - \varepsilon_{x,0}(c_r = 0.27)}{\varepsilon_{x,0}(c_r = 0.27)}$$

The values of $\Delta\varepsilon_{x,0}(c_r)$ are given in Tab. 3 for each configuration and also given as contour plot in Fig. 7. The straight-wing configuration (Λ_{LE} = 6°) shows the largest values of $\Delta\varepsilon_{x,0}(c_r)$ because in this case the reference pre-strain by c_r = 0.27 is relatively low compared to the other configurations.

4.2 Wing Geometries

4.2.1 Airfoil Shapes

The stereo-photogrammetry measurements performed on the upper and on the lower wing surfaces were combined in order to analyze the airfoil shapes resulting from the deformation of the membrane. In the following, only the airfoil sections measured at a spanwise station corresponding to y/b = 0.3 are considered, which is the station around which the maximum deflection was measured in all cases as will be shown later. The results are shown in Fig. 8, Fig. 9, and Fig. 10 for the straight-wing (Λ_{LE} = 6°), for the intermediate (Λ_{LE} = 30°), and for the swept-back configurations (Λ_{LE} = 43°), respectively. Each of the diagrams highlight the impact of the variation of the pre-tension on the airfoil shapes at α = 10° for a given free-stream dynamic pressure.
The large dependency of the airfoil shapes on the free-stream dynamic pressure already known from previous investigations (see Fig. 2) can effectively be compensated to some extent by varying the pre-tension of the membrane. A comparison between the airfoil shapes measured on the three wing configurations shows that the overall largest deflections occur in the case of the straight-wing configuration and the smallest in the case of the intermediate configuration. The swept-back configuration shows deflection amplitudes somewhere in between. This follows exactly the trend of $\varepsilon_{x,0}$ observed in Fig. 7 which, comparing only the three configurations considered here, is minimum for Λ_{LE} = 6° and maximum for Λ_{LE} = 30°. It indicates also that the spanwise pre-strain $\varepsilon_{y,0}$ has not a significant influence on the deformation. Further, the range of airfoil cambers that can be achieved while moving the trailing-edge reflects well the relative variation of the pre-strain $\Delta\varepsilon_{x,0}(c_r)$ shown in Fig. 7 and Tab. 3. In fact, the broadest range of airfoils shapes is obtained for the straight-wing configuration (Λ_{LE} = 6°), which also has the largest values of $\Delta\varepsilon_{x,0}(c_r)$, whereas the narrowest range of airfoil shapes is obtained in the case of the intermediate configuration accordingly.

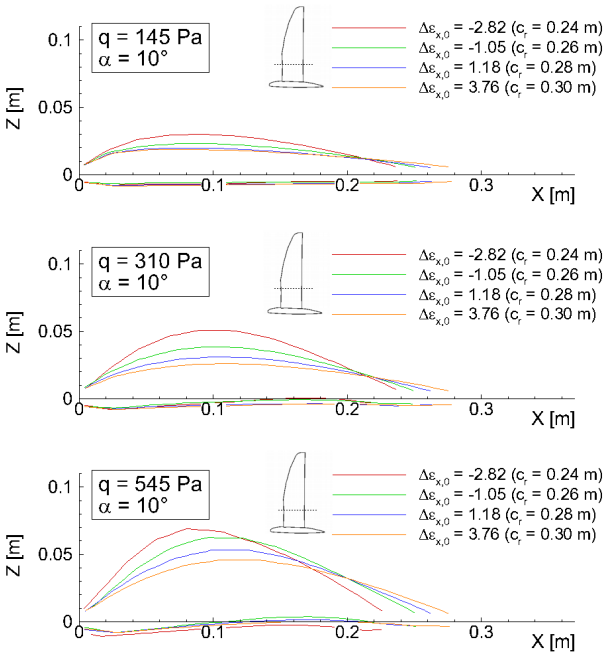

Fig. 8 Airfoils shapes of the straight-wing configuration (Λ_{LE} = 6°).

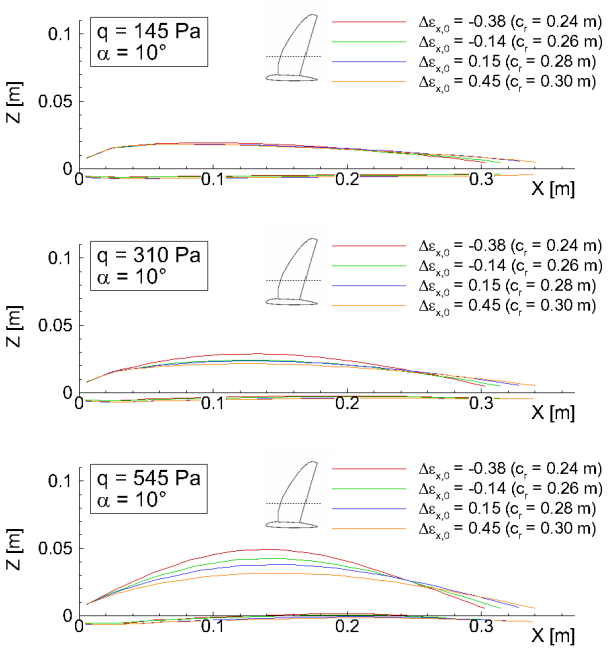

Fig. 9 Airfoils shapes of the intermediate wing configuration (Λ_{LE} = 30°).

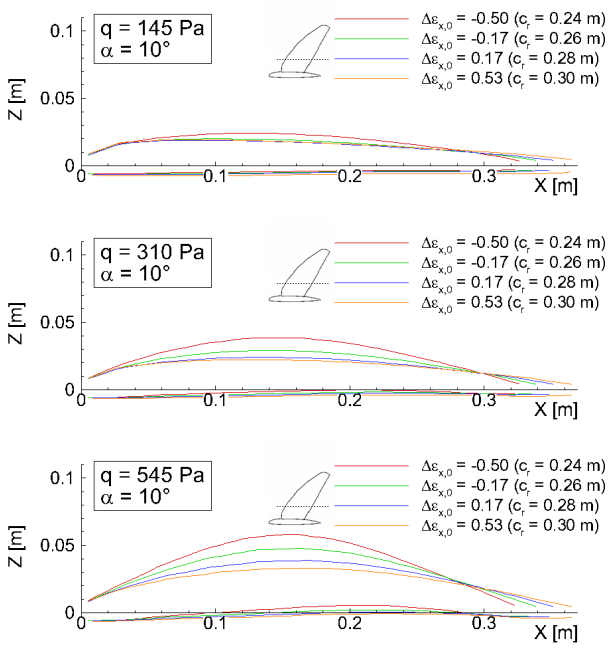

Fig. 10 Airfoils shapes of the swept-back wing configuration (Λ_{LE} = 43°).

4.2.2 Spanwise Camber Distribution

Figure 11 shows the spanwise camber distributions (relative camber f) of the straight-wing, intermediate and swept-back configurations. The results are only given for q = 310 Pa and α = 10°, but similar trends were observed in all other cases. All camber distributions show similar shapes with the maximum located between y/b = 0.3 and y/b = 0.4. The variation in spanwise camber distribution reflects well the trends observed while analyzing th airfoil shapes. In fact, the straight-wing configuration shows the largest absolute camber as well as the broadest range of cambers, while the intermediate configuration has the smallest cambers.

4.3 Aerodynamic Performances

The previous section illustrated how the chordwise pre-tension influences the wing camber. Here, the resulting effect on the aerodynamic performance of the wing obtained from the force measurements is discussed.

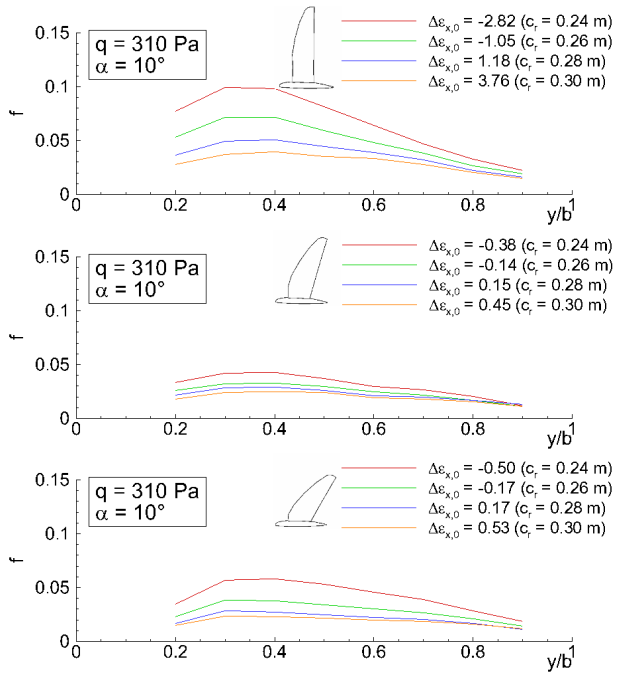

Fig. 11 Spanwise camber distributions.

4.3.1 Lift

The geometry variation resulting from an increase of the root chord parameter c_r is twofold. On the one hand it slightly increases the wing area (see Fig. 4), and on the other hand, it reduces the wing camber (see Fig. 11). Since both effects have opposite influence on the lift, the net effect depends on the relative influence of both aspects. The diagrams of Fig. 12 shows the lift curves obtained for the straight-wing, the intermediate and the swept-back configurations at free-stream dynamic pressure q = 310 Pa. All lift coefficients are based on a common average reference area in order to address the influence of c_r on the real lift production. Using the reference area of each configuration would filter out the influence of the changing wing area. In the case of the straight-wing configuration, the lift curve slope clearly decreases with increasing c_r , meaning that the varying camber induces a larger variation of the lift than the varying wing area. This tendency is also observed in the case of the swept-back configuration, however, it is less pronounced as a result of the narrower range of wing cambers achieved in this case compared to the straight-wing configuration (see Fig. 11).

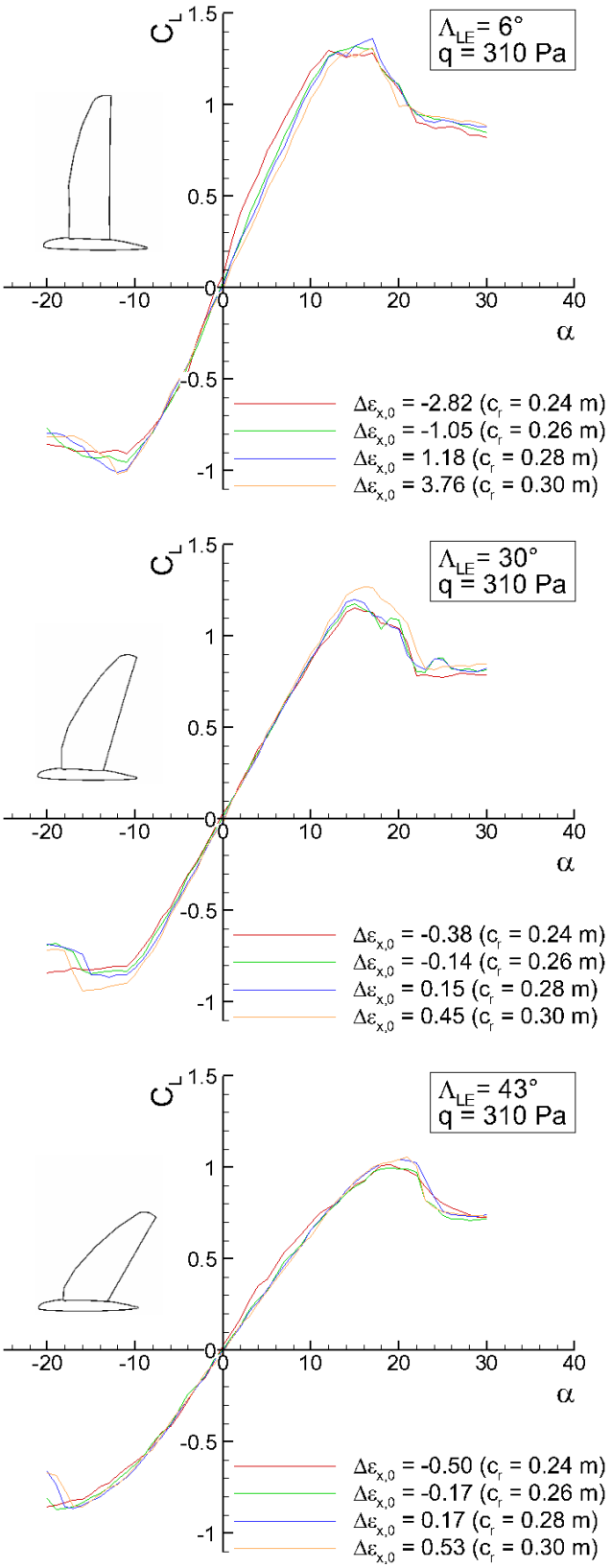

Fig. 12 Lift characteristics.

The lift characteristics of the intermediate configuration show no significant dependency on c_r , because the very small variation in camber is compensated by the changing wing area. Finally, the slope of the lift curves decreases while the planform shape changes from the straight-wing to the swept-back configurations as a result of the decreasing aspect ratio.

4.3.2 Lift-to-Drag Ratio

The diagrams of Fig. 13 highlight the influence of the chordwise pre-tension on the maximum lift-to-drag ratio $(L/D)_{max}$ as function of the free-stream dynamic pressure for the three wing configurations considered. Clearly, the pre-tension has a significant influence on $(L/D)_{max}$ as a result of its effect on the wing camber. At the lowest dynamic pressure (q = 145 Pa), the optimum values of $(L/D)_{max}$ are always reached with the lowest pre-tension investigated, i.e., by setting c_r = 0.24 m. In this case, a small pre-tension is required to allow the low aerodynamic loading to morph the airfoil into a more efficient shape than the undeflected one. In contrast, the best $(L/D)_{max}$ are obtained using larger pre-tension at higher free-stream dynamic pressure, because larger pre-tensions prevent massive deflections which result in inefficient airfoil shapes. In fact, when the camber becomes excessively large the flow begins to separate at the trailing-edge and the drag increases as a result. Comparing now the three planform configurations among each other, the straight-wing shows the overall highest lift-to-drag ratios accordingly to its large aspect ratio with optimum $(L/D)_{max}$ at a given dynamic pressure between 17 and 18. The range of $(L/D)_{max}$ then globally decreases with decreasing aspect ratio as expected. In fact, the intermediate configuration has optimum $(L/D)_{max}$ values between 15 and 17, and finally the swept-back configuration has the lowest optimum $(L/D)_{max}$ values between 13.5 and 14.5. Further, $(L/D)_{max}$ values interpolated for $\Delta\varepsilon_{x,0}(c_r) = 0$, i.e., the case of a fixed trailing-edge with a root chord of c_r = 0.27 m, are compared in Fig. 14 to the best $(L/D)_{max}$ obtained by ad-

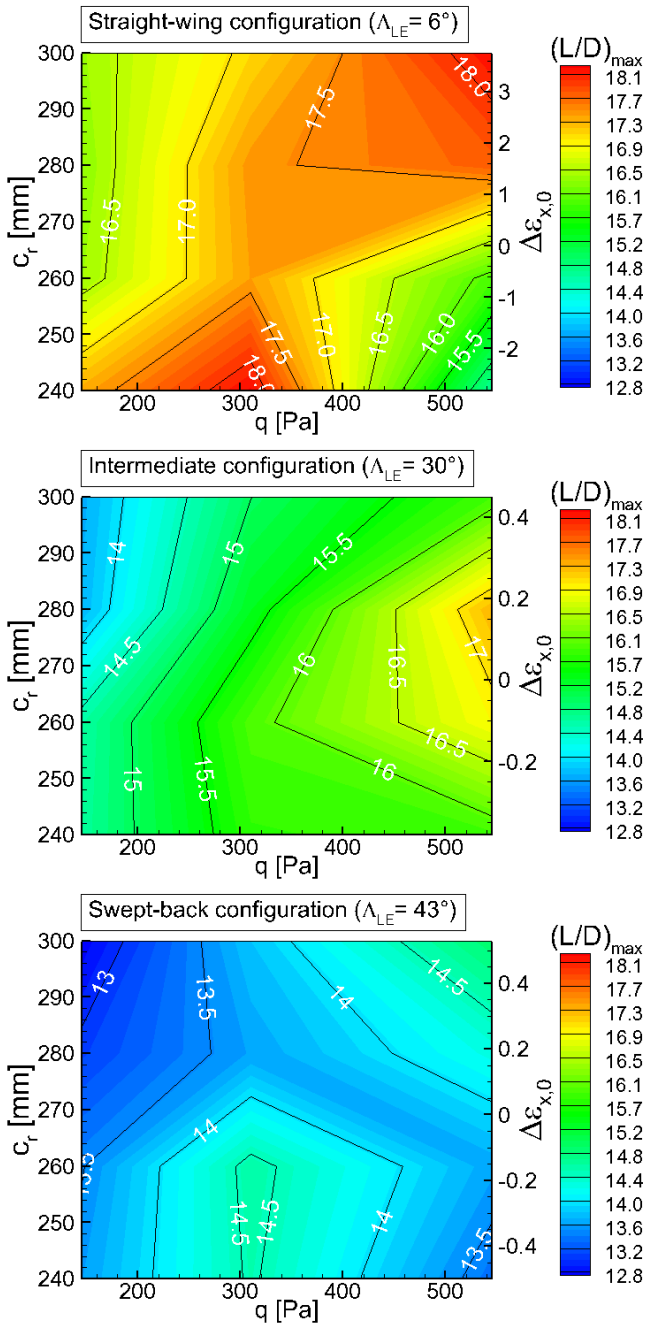

Fig. 13 Effect of a modification of the pre-tension on the maximum lift-to-drag ratio at different dynamic pressures.

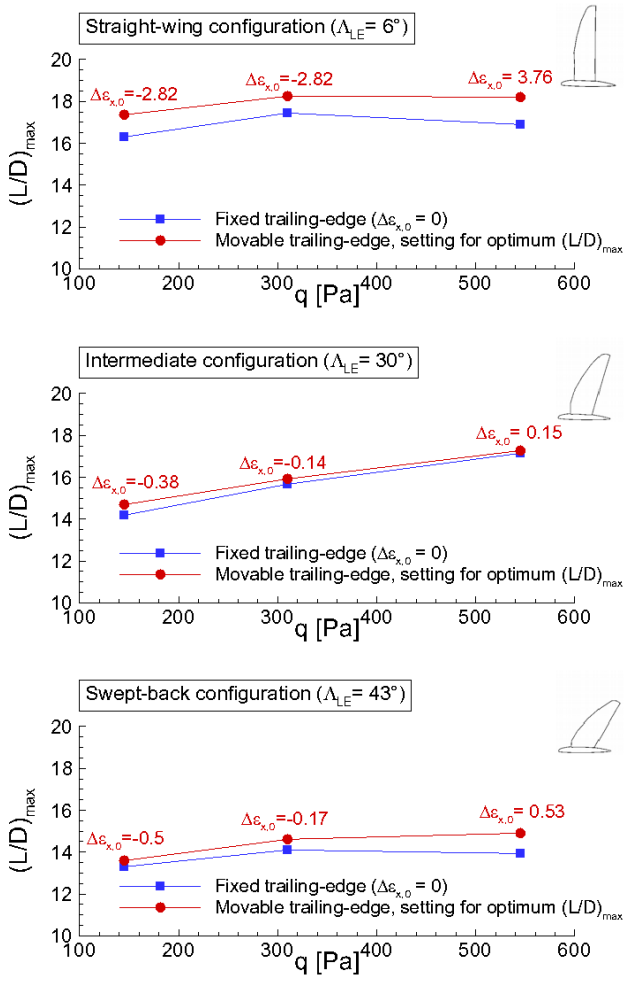

Fig. 14 Maximum lift-to-drag ratio versus free-stream dynamic pressure with and without active control of the pre-tension.

justment of the pre-tension at each free-stream dynamic pressure. The respective pre-tension settings for which those optimum $(L/D)_{max}$ are reached are given in the diagrams by $\Delta\varepsilon_{x,0}(c_r)$. Clearly, the active control of the pre-tension effectively allows improving the lift-to-drag ratio at a given free-stream dynamic pressure compared to a case where the membrane just passively reacts to the varying flow conditions.

5 Conclusion and Outlook

This paper presented the experimental investigations on a morphing membrane wing allowing large modifications in planform shape and wing camber. The analysis focused on the control of the passive deformation of the flexible wing surface to control the wing camber. For this, a wind tunnel model using a movable trailing-edge allowing for an active variation of the pre-tension of the membrane was investigated. The experimental results based on stereo-photogrammetry measurements demonstrated that the wing camber can be effectively adjusted within a certain range at a given flow condition by modifying its pre-tension. At the same time, the mean amplitude of the wing camber as well as the reachable range of cambers depend on the planform shape because its variation intrinsically influences the mean level of pre-tension. The results of the force measurements showed that the performances of the wing can be effectively altered by modifying the pre-tension, as a direct result of the modified wing camber. For instance, it was shown that the lift-to-drag ratio can be significantly improved at a given free-stream dynamic pressure compared to the case where the wing surface just passively deforms.

Future work will still focus on the development of methods to control the deformation of the membrane and further optimize the performance of the wing. This will mainly include the design of a membrane material with specific anisotropic properties, which can be used to obtain a predefined camber distribution. For this, further experimental tests as well as numerical simulations are planned.

References

[1] Moorhouse, D., Sanders, B., von Spakovsky, M., and Butt, J., *Benefits and Design Challenges of Adaptive Structures for Morphing Aircraft*. The Aeronautical Journal, Paper No. 3012, 2006, pp. 157-162

[2] Thill, C., Etches, J., Bond, I., Potter, K., and Weaver, P., *Morphing Skins*. The Aeronautical Journal, Vol. 112, No. 1129, 2008, pp. 117-139.

[3] Rodriguez, A. R., *Morphing Aircraft Technology Survey*. 45^{th} AIAA Aerospace Sciences Meeting and Exhibit, Reno, Nevada, Jan. 8-11, 2007, AIAA-2007-1258.

[4] Pendelton, E., Flick, P., Donald, P., Voracek, D.,Reichenbach, E., Griffin, K., *The X-53 - A Summary Of The Active Aeroelastic Wing Flight Research Program*. 48^{th} AIAA/ASME/ASCE/AHS/ASC Structures, Structural Dynamics, and Materials Conference, Honolulu, Hawaii, April. 23-26, 2007.

[5] Muray, H., and Maruyama, S., *Theoretical Investigation of Sailwing Airfoils Taking Account of Elasticities*. *Journal of Aircraft*, Vol. 19, No. 5, 1982, pp. 385, 389. doi: 10.2514/3.44762.

[6] Béguin, B., Breitsamter, C., and Adams, N., *Aerodynamic Investigations of a Morphing Membrane Wing*. AIAA Journal, J051772 (accepted).

[7] Luhmann, T., Robson, S., Kyle, S., and Harley, I., *Close Range Photogrammetry*. Whittles Publishing, 1^{st} ed., 2006.

Copyright Statement